SCIENCE CHINA
Technological Sciences

December 2011 Vol.54 No.12: 3180–3190
doi: 10.1007/s11431-011-4606-7

Analytical modeling of geometric errors induced by cutter runout and tool path optimization for five-axis flank machining

GUO Qiang, SUN YuWen* & GUO DongMing

Key Laboratory for Precision and Non-Traditional Machining Technology of the Ministry of Education, Dalian University of Technology, Dalian 116024, China

Received August 24, 2011; accepted September 7, 2011; published online November 5, 2011

The cutter runout effect has significant influence on the shape of cutter swept surface and the machining surface quality. Hence, it is necessary to integrate the cutter runout effect in cutter swept surface modeling, geometric error prediction and tool path optimization for five-axis flank machining. In this paper, an envelope surface model considering cutter runout effect is first established, and geometric errors induced by runout effect are derived based on the relative motion analysis between the cutter and part in machining. In the model, the cutter runout is defined by four parameters, including inclination angle, location angle, offset value and the length of cutter axis. Then the runout parameters are integrated into the rotation surface of each cutting edge that is used to form the final cutter envelope surface for the five-axis machining process. Thus, the final resulting geometric errors of the machined surface induced by cutter runout can be obtained through computing the deviations from the nominal cutter swept surface. To reduce these errors, an iterative least square method is used to optimize the tool paths for five-axis flank machining. Finally, a validation example is given for a specific ruled surface. Results show the effectiveness and feasibility of the analytical model of geometric errors induced by cutter runout, and also show that the geometric errors can be reduced significantly using the proposed tool path planning method.

cutter runout, tool path optimization, envelope surface, five-axis machining, geometric errors

Citation: Guo Q, Sun Y W, Guo D M. Analytical modeling of geometric errors induced by cutter runout and tool path optimization for five-axis flank machining. Sci China Tech Sci, 2011, 54: 3180–3190, doi: 10.1007/s11431-011-4606-7

1 Introduction

Five-axis flank machining process is broadly used in manufacture industries such as automotive, aeronautic and aerospace field. With the two degrees of additional freedom of rotation, it has the ability to expand the process ranges and improve the machining quality and efficiency. Currently, some works have been focused on the five-axis flank machining process including tool path optimization [1–7], cutting forces prediction or detection [8–10], cutting process simulation [11–13] and machining chatter [14, 15].

In five-axis flank machining, modeling the cutter envelope surface is an important aspect since it can be used to predict geometric error and optimize tool paths. Among many methods of modeling envelope surface, Wang et al. [16] proved that the velocity of a point on the envelope surface must be perpendicular to the normal of the surface on this point. This is the key to obtain the envelope surface of cutter. Sheltami et al. [17] used the generating curve to model the sweep surface of cutter in five-axis milling process. They proposed that the swept surface is the trace of the generating curves. In the model they assumed that the motion of cutter between two successive cutter positions is linear, meanwhile the cutter axis always lies in one plane. Blackmore et al. [18] obtained the swept surface of a cutter

*Corresponding author (email: xiands@dlut.edu.cn)

in five-axis milling by numerically solving the sweep-envelope surface differential equation. Aras [19] presented an approach to determine the shape of envelope surface utilizing the families of spheres with two parameters. Generally, cutter swept surface modeling has been researched from different aspects in the existing literature. The envelope surface can be generated with a high accuracy. However, the cutter runout effect has never been considered in the existing envelope surface models. Actually, to some extent the cutter runout effect is very common and inevitable in five-axis milling process. The reason of this is that there have the misalignments, the manufacturing or wear error of cutter and so on. For the cutter runout has significant influence on the machining quality and process geometry parameters, both the shape and position of envelope surface have had changes compared with the ideal cutter swept surface without cutter runout. It is necessary to integrate the cutter runout effect into the cutter swept model.

In the aspect of tool path planning for five-axis flank machining, most of existing works focused on reducing geometric errors aroused from the approximation of non-developable ruled surface. For example, Liu [20] presented a method which is able to compute cutter location fast. In this method, they took two points on a rule with parameter values of 0.25 and 0.75, then offset these two points along the normal vector of the surface with a distance of the cutter radius, the cutter axis was finally determined. Bedi et al. [21] noted the case where only two curves on the machined surface are known and the shape of the surface is to be determined by a tool sliding along the generating rails. After giving a detailed mathematical understanding of flank milling with flat end cutters, a method was proposed by sliding the cutter along two rails and keeping the cutter tangent to both curves at every parameter value. For small tool steps the machined surface may be an acceptable approximation to a ruled surface. In addition, Senatore et al. [22] optimized the tool path through positioning the tool axis using envelope surface. When necessary, Lartigue et al. [5] utilized the strategy of tool path deformation to make the envelope surface fit the ideal surface as much as possible. Further, Gong [23] first optimized tool paths by a envelope surface approximation using global optimization and the results inspired researchers to plan tool paths from local view to global view. Zhu and Ding et al. [3, 4] first used the third-order point contact principle to optimize the tool path surface and improved the approximation accuracy significantly. Also, a global optimization method following the minimum zone criterion is presented [1, 24]. From these we can see that great efforts have been done on tool path planning for flank machining. On the other hand, the cutter runout can cause the fluctuation of magnitudes of cutting forces [9, 25], and such fluctuations as well as geometric errors induced by cutter runout can be reduced significantly if the cutter runout is compensated in tool path planning. However, it is still not concerned in the existing literature.

In this paper, the analytic model of geometric errors induced by cutter runout effect is researched, and subsequently a tool path planning method is proposed to reduce the geometric errors and cutting force fluctuations aroused by cutter runout. To systematically investigate the influences of cutter runout in theory, the cutter runout defined in the paper not only contains parallel axis error which is often considered in engineering and existing literature, but also contains inclination angle errors of the cutter axis relative to the nominal cutter axis.

2 Relative motion analysis of cutter-part considering cutter runout effect

For a tapered-helical-ball-end mill as shown in Figure 1, the equation of the kth cutting edge can be expressed using the following equation

If $z>0$

$$\begin{cases} x_c(z) = r\cos\left(\dfrac{\tan(\beta)\ln\left(r/R_0\right)}{\sin(\xi/2)} + \dfrac{2(k-1)\pi}{N}\right), \\ y_c(z) = r\sin\left(\dfrac{\tan(\beta)\ln\left(r/R_0\right)}{\sin(\xi/2)} + \dfrac{2(k-1)\pi}{N}\right), \\ z_c(z) = z, \\ r = \left(R_0 + z\tan\left(\dfrac{\xi}{2}\right)\right). \end{cases} \quad (1)$$

Else

$$\begin{cases} x_c(z) = r\cos\left(\dfrac{\tan(\beta)\ln\left(\left(R_0+z\right)/\left(R_0-z\right)\right)}{2} + \dfrac{2(k-1)\pi}{N}\right), \\ y_c(z) = r\sin\left(\dfrac{\tan(\beta)\ln\left(\left(R_0+z\right)/\left(R_0-z\right)\right)}{2} + \dfrac{2(k-1)\pi}{N}\right), \\ z_c(z) = z, \\ r = \sqrt{R_0^{\,2} - z^2}, \end{cases} \quad (2)$$

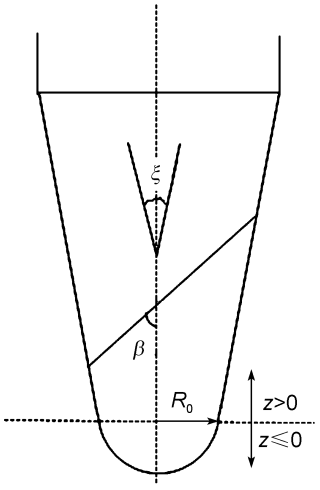

Figure 1 The tapered-helical-ball-end mill.

where the radius of the cone roof is R_0, ξ is the whole conical angle of the cone roof, N is the number of the cutting edges and β is the helix angle of the cutter.

In five-axis flank machining, the cutting edges rotate about the spindle axis not the cutter axis. When cutter runout effect does not exist under ideal machining status, the axis of cutter is coincident with the spindle axis. However, when the cutter runout effect in milling process appears, the axis of the rotation surface of cutting edge should turn from the cutter axis to the spindle axis. To investigate the influence of cutter runout, the cutter runout parameters should be first defined. As the most complicated situations, the deviations of rotation and transformation of the cutter axis relative to the machining spindle axis are both considered as shown in Figure 2. This means the defined cutter runout errors are a combination of parallel axis error and inclination angle error.

For the cutter runout with most complex status, four parameters can be used to define runout errors, namely offset ρ, inclination angle γ, the length of cutter axis l_c, and the location angle λ. Details about the definitions of these parameters are as follows:

• offset ρ: the common normal length between the cutter axis and spindle axis.

• inclination angle γ: the included angle between the cutter axis and spindle axis.

• the length of cutter axis l_c: the length between the bottom of cutter axis (z=0) and the intersection point of the common normal line and cutter axis.

• location angle λ: the intersection angle between the vector of O_cO_i and the first cutting edge direction vector passing through the first cutting edge point and point O_c as illustrated in Figure 3.

In five-axis milling process with cutter runout effect, the cutting edge is rotating about spindle axis not the cutter axis. As seen in Figure 3 two coordinate systems are introduced, the first one is the cutter coordinates system $\{O_c, X_c, Y_c, Z_c\}$, and the second one is the rotation coordinate system $\{O_r, X_r, Y_r, Z_r\}$. Thus, eqs. (1) and (2) are first established in the cutter coordinate system, then the cutting edge equation should be turned into the coordinate system of rotation.

The details of rotation coordinate system are given as follows. The Z_r-axis of rotation coordinate system is the axis of machine spindle. When the Z_r-axis of coordinate system $\{O_r, X_r, Y_r, Z_r\}$ is parallel to the corresponding axis of the workpiece coordinate system, the X_r-axis of coordinate system $\{O_r, X_r, Y_r, Z_r\}$ is also parallel to the corresponding axis of the workpiece coordinate system. The origin of coordinate system $\{O_r, X_r, Y_r, Z_r\}$ is chosen based on the following rules. At the bottom of cutter axis (z=0), a plane perpendicular to the cutter axis can be constructed as seen in Figure 2. Passing through the intersection point of the spindle axis and the common normal line between the cutter axis and spindle axis, a line parallel to the cutter axis

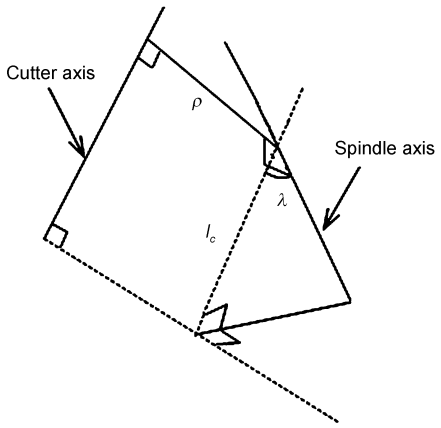

Figure 2 Runout definition.

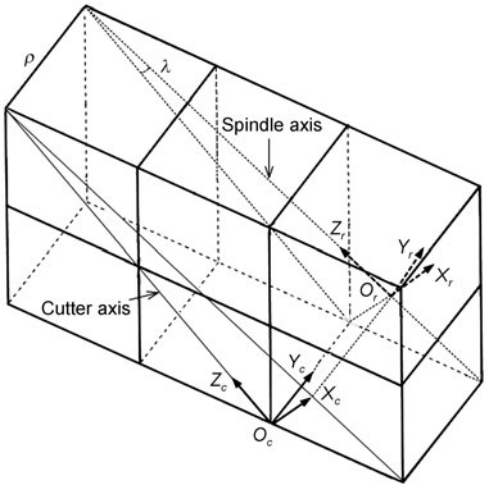

Figure 3 Coordinate systems of the cutter and the rotation.

is constructed. Then another straight line perpendicular to the auxiliary line as well as intersecting with the spindle axis is built. Thus, the intersecting point is just the origin of coordinate system $\{O_r, X_r, Y_r, Z_r\}$.

The cutter coordinate system is defined with the following details. The Z_c-axis of cutter coordinate system is the axis of cutter. The Y_c-axis of coordinate system $\{O_c, X_c, Y_c, Z_c\}$ is parallel to the vector product between spindle axis (Z_r–axis of the $\{O_r, X_r, Y_r, Z_r\}$) and cutter axis (Z_c-axis of $\{O_c, X_c, Y_c, Z_c\}$). And X_c-axis of coordinate system $\{O_c, X_c, Y_c, Z_c\}$ is parallel to the vector product between Y_c-axis and Z_c-axis axes of $\{O_c, X_c, Y_c, Z_c\}$. The origin of $\{O_c, X_c, Y_c, Z_c\}$ is chosen at the bottom of cutter axis (z=0) as shown in Figure 3.

An arbitrarily given point $\boldsymbol{P}_r$ on the cutting edge in coordinate system $\{O_c, X_c, Y_c, Z_c\}$ can be expressed in $\{O_r, X_r, Y_r, Z_r\}$ using the following equation:

$$\boldsymbol{P}_r = \boldsymbol{L}_r + \boldsymbol{E}(\boldsymbol{P}_p + \boldsymbol{L}_c) = [\boldsymbol{l}_{rx} \quad \boldsymbol{l}_{ry} \quad \boldsymbol{l}_{rz}]^{\mathrm{T}}, \tag{3}$$

where

$$\boldsymbol{L}_c = \{0\ 0\ -\boldsymbol{l}_c\}^{\mathrm{T}},$$

$$\boldsymbol{L}_r = \left\{0\ 0\ \boldsymbol{l}_c \middle/ \cos(\gamma)\right\}^{\mathrm{T}},$$

$$\boldsymbol{E} = \begin{Bmatrix} \cos\gamma\cos\alpha_0 & -\sin\alpha_0 & \sin\gamma\cos\alpha_0 \\ \cos\gamma\sin\alpha_0 & \cos\alpha_0 & \sin\gamma\sin\alpha_0 \\ -\sin\gamma & 0 & \cos\gamma \end{Bmatrix},$$

and

$$\boldsymbol{P}_p = \begin{Bmatrix} x_p \\ y_p \\ z_p \end{Bmatrix} = \begin{Bmatrix} r\cos(\theta+\lambda) \\ r\cos(\theta+\lambda)-\rho \\ z \end{Bmatrix}, \tag{4}$$

while $z >= 0$ $\theta = \dfrac{\tan(\beta)\ln(r/R_0)}{\sin(\xi/2)} + \dfrac{2(k-1)\pi}{N}$,

else $\theta = \dfrac{\tan(\beta)\ln\left((R_0+z)/(R_0-z)\right)}{2} + \dfrac{2(k-1)\pi}{N}$.

From eqs. (3) and (4), we can see that when the inclination angle is zero, the cutter runout error is turned into the parallel axis error. When the offset parameter is zero, the runout error is completely aroused by the inclination angle error. The parameter α_0 is defined as the initial angle. The initial angle is the included angle between X_c-axis of $\{O_c, X_c, Y_c, Z_c\}$ and X_r-axis of $\{O_r, X_r, Y_r, Z_r\}$. In Figure 3, the initial angle is zero. In five-axis flank milling process, a different machine type has a different kinematic pattern. Usually, five-axis machine tools have three types: 5-axis with dual rotary head machine, 5-axis with dual rotary table machine and 5-axis with rotary head and table machine. Here takes the second type to analyze the relative motion relationships between the cutter and part. The configuration of this type of five-axis machine is shown in Figure 4.

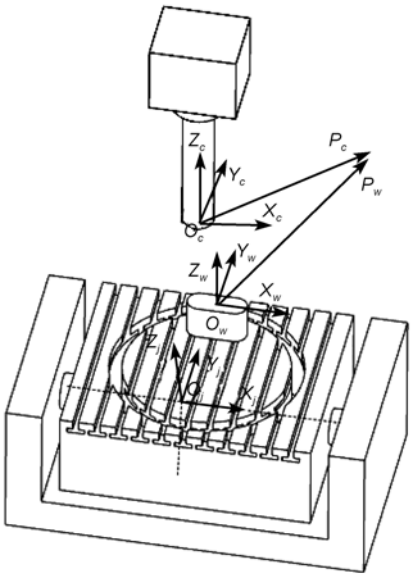

Figure 4 Dual rotary table machine coordinate systems.

In Figure 4, three coordinate systems are illustrated. The relative motion of the cutter and part can be described using the translation motion of rotation coordinate system in the pivot coordinate system and the rotation motion of the pivot coordinate system in the workpiece coordinate system. Here, the pivot coordinate system is defined as $\{O_j, X_j, Y_j, Z_j\}$ and the workpiece coordinate system is defined as $\{O_w, X_w, Y_w, Z_w\}$. Then the point on the cutting edge in eq. (3) can be expressed in $\{O_w, X_w, Y_w, Z_w\}$ using the following equations:

$$\boldsymbol{P}_w = \boldsymbol{r}_m + \boldsymbol{T}(\gamma)\boldsymbol{T}(\alpha)\left(\boldsymbol{r}_s - \boldsymbol{r}_m + \boldsymbol{P}_r\right), \tag{5}$$

where $\boldsymbol{r}_m = \boldsymbol{O}_j - \boldsymbol{O}_w$, $\boldsymbol{T}(\gamma)$ and $\boldsymbol{T}(\alpha)$ are counterclockwise unit rotation matrixes about Z_j-axis and X_j-axis respectively. α and γ are tilt angles about X_j-axis and Z_j-axis axes respectively and can be calculated utilizing the cutter axis vector at time t. $\boldsymbol{r}_s$ is the vector between the current position and the initial position of the origin of cutter coordinate system. The rotation surface for the kth cutting edge can be expressed using the following equation:

$$\boldsymbol{P}_{we}(k,\theta,z) = \boldsymbol{r}_m + \boldsymbol{T}(\gamma)\boldsymbol{T}(\alpha)\left(\boldsymbol{r}_s - \boldsymbol{r}_m + \boldsymbol{B}(\theta)\boldsymbol{P}_r\right) \quad \text{with} \quad \theta \in [0, 2\pi], \tag{6}$$

where $\boldsymbol{B}(\theta)$ is counterclockwise unit rotation matrix about x-axis

When the cutter runout effect exists, all cutting edges will not rotate about the cutter axis but the spindle axis. In this case, the rotation surface of each cutting edge is different from others. This means, the number of rotation surfaces formed by cutting edges is no longer one and equal to the number of cutting edges. Meanwhile, even in the case where the runout error is only parallel axis error, the rotation surfaces formed by different generating lines are also different. As shown in Figure 5, when the generating line is selected a straight line parallel to the cutter axis, the rotation surface is still cylindrical surface under existing parallel axis error, while it is a complex surface when a cutting edge is used as the generating line. This is the reason why the

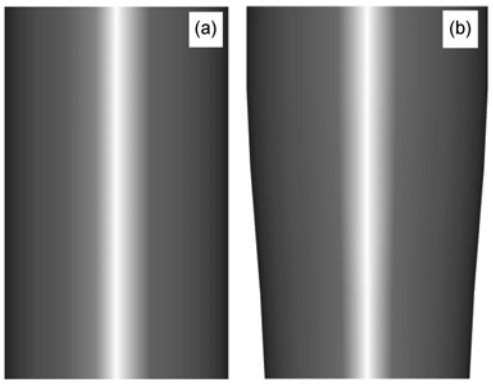

Figure 5 Rotation surface formed by different generating lines. (a) Straight line; (b) cutting edge.

cutting edges are selected as generating lines of rotation surface to derive the resulting envelope surface.

3 Envelope surface generation

In five-axis milling process, the tool path in the APT file is given by a series of cutter position points and corresponding cutter-axis vectors $\{\boldsymbol{Q}_i\, \boldsymbol{a}_i\}$. Figure 6 shows a part of an APT file derived from UG5.0 software. From Figure 6, the data in green frame are the cutter position point and the data in red frame are the corresponding cutter-axis vectors. And both frames contain three volume data standing for cutter position points' components and cutter axis vectors' components along the three-axis directions of the workpiece coordinate system. For i_{th} row, the cutter position point and the corresponding cutter axis vector can be formed as the following expressions:

$$\left\{\boldsymbol{Q}_i, \boldsymbol{a}_i\right\} = \left\{x, y, z, a_x, a_y, a_z\right\}, \tag{7}$$

where $\boldsymbol{Q}_i$ is the i_{th} cutter position point and $\boldsymbol{a}_i$ is the corresponding cutter axis vector. x, y and z are the components of cutter position point along x, y and z axes in workpiece coordinate system. a_x, a_y and a_z are the corresponding components of the cutter axis vector. Actually, the tool path surface is a ruled surface. To accurately express the tool path surface, this ruled surface can be modeled using B-spline surface. If the tool path is constructed by a series of points illustrated in Figure 5, two B-spline curves can also be constructed by interpolating or approximating the given data points. Without losing generality, the tool path surface can be expressed as

$$\boldsymbol{sf}_w(u,v) = (1-v)\sum_{i=0}^{n} N_{i,3}(u)\boldsymbol{b}_{\text{Boti}} + v\sum_{i=0}^{n} N_{i,3}(u)\boldsymbol{b}_{\text{Topi}} \quad \text{with} \quad u \in [0,1], v \in [0,1], \tag{8}$$

where $\boldsymbol{b}_{\text{Boti}}$ is the i_{th} control point of the curve on the tool path surface at the bottom of cutter. $\boldsymbol{b}_{\text{Topi}}$ is the i_{th} control point of the curve on the tool path surface at the top of cutter as shown in Figure 7.

For the cutter envelope surface, if a point is on the envelope surface, it is also on the rotation surface about the spindle axis of the cutting edge. And when a point on the rotation surface of the cutting edge is also on the envelope surface, a condition should be met that the relative velocity vector of the point must be perpendicular to the normal vector of the rotation surface of the cutting edge at the position of the point. Theoretically, the conjugation condition of two surfaces can be expressed as

$$\boldsymbol{n}_p(k,\theta,z)\cdot\boldsymbol{V}_p(\theta,v) = 0, \tag{9}$$

where $\cdot$ stands for the scalar product between two vectors. $\boldsymbol{n}_p(k,\theta,z)$ is the normal vector at point $\boldsymbol{p}$ (kth cutting edge, at angle of θ and at the height of z). $\boldsymbol{V}_p(\theta, v)$ is the velocity at the point $\boldsymbol{p}$. The relationship between z and v can be expressed as

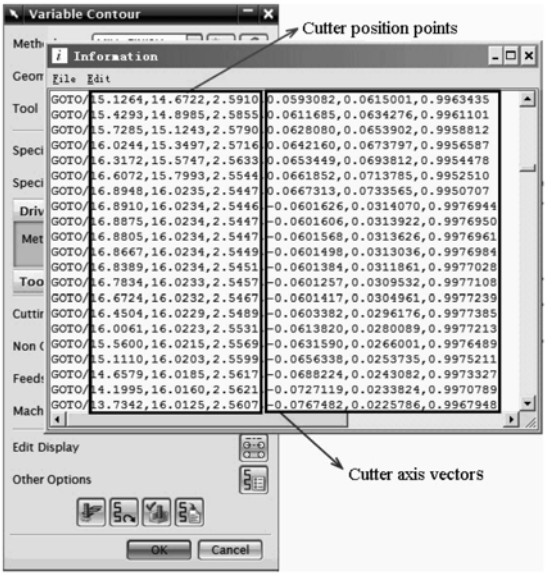

Figure 6 The tool path in APT file.

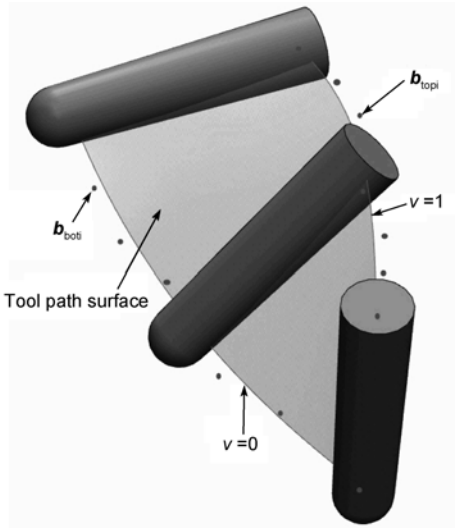

Figure 7 Tool path surface and corresponding control points.

$$v = z \Big/ \left\|\boldsymbol{b}_{\text{Topi}} - \boldsymbol{b}_{\text{Boti}}\right\|. \tag{10}$$

As illustrated in Figure 1, when z<0, the parameter v in eq. (10) is less than zero. This will lead to conflict with v in eq. (8) in which v belongs to [0, 1]. A method is given to avoid this confliction. That is to move cutter position points from tool center points to tool tip points. Then the $\boldsymbol{b}_{\text{Boti}}$ can be derived though interpolating tool tip points. Eq. (10) is turned into

$$v = (z + R_0) \Big/ \left\|\boldsymbol{b}_{\text{Topi}} - \boldsymbol{b}_{\text{Boti}}\right\|. \tag{11}$$

The normal vector at point $\boldsymbol{p}$ can be constructed as

$$\boldsymbol{n}_p(k,\theta,z)=\frac{\partial \boldsymbol{P}_{we}(k,\theta,z)}{\partial\theta}\times\frac{\partial \boldsymbol{P}_{we}(k,\theta,z)}{\partial z}, \tag{12}$$

where × stands for vector product between two vectors. Using eq. (6), the partial derivatives with respect to θ and z can be expressed using

$$\begin{cases}\dfrac{\partial \boldsymbol{P}_{we}(k,\theta,z)}{\partial\theta}=\boldsymbol{T}(\gamma)\boldsymbol{T}(\alpha)\left(\dfrac{\mathrm{d}\boldsymbol{B}(\theta)}{\mathrm{d}\theta}\boldsymbol{P}_r\right),\\ \dfrac{\partial \boldsymbol{P}_{we}(k,\theta,z)}{\partial z}=\boldsymbol{T}(\gamma)\boldsymbol{T}(\alpha)\boldsymbol{B}(\theta)\dfrac{\mathrm{d}\boldsymbol{P}_r}{\mathrm{d}z}.\end{cases} \tag{13}$$

Then the cutter axis vector at the u position of tool path can be constructed according to the curve $\boldsymbol{sf}_w(u,1)$ and $\boldsymbol{sf}_w(u,0)$. That is

$$\boldsymbol{a}(u)=\left(\boldsymbol{sf}_w(u,1)-\boldsymbol{sf}_w(u,0)\right)\Big/\left\|\boldsymbol{sf}_w(u,1)-\boldsymbol{sf}_w(u,0)\right\|, \tag{14}$$

where $\boldsymbol{a}(u)$ is the cutter axis vector at position u. Using this vector, the tilt angles about x and z axes can be calculated. The translational and rotational velocities at position u as well as the velocity at the point (k, θ, z) can be computed using

$$\begin{cases}\boldsymbol{V}(u)=\mathrm{d}\boldsymbol{sf}_w(u,0)/\mathrm{d}u,\\ \boldsymbol{\omega}(u)=\boldsymbol{a}(u)\times\mathrm{d}\boldsymbol{a}(u)/\mathrm{d}u,\\ \boldsymbol{V}(u,\theta,v,k)=\boldsymbol{V}(u)+\boldsymbol{\omega}(u)\times\boldsymbol{P}_{we}(k,\theta,z).\end{cases} \tag{15}$$

After substituting eqs. (15) and (13) into eq. (9), the parameter θ at the height of z for k_{th} cutting edge can be computed. Then substituting (k, θ, z) into eq. (6), can lead to the point on the envelope surface. Using this method an envelope surface point is given in $\{O_w, X_w, Y_w, Z_w\}$. Here another method is proposed, that is to compute the point in $\{O_r, X_r, Y_r, Z_r\}$ and then transform the point from $\{O_r, X_r, Y_r, Z_r\}$ to $\{O_w, X_w, Y_w, Z_w\}$. The advantage of the method is that the expression of θ is simplified.

For parameter θ, the following steps are adopted to compute parameter θ at the height of z for k_{th} cutting edge. Firstly, transform the velocity of eq. (15) in $\{O_w, X_w, Y_w, Z_w\}$ to $\{O_r, X_r, Y_r, Z_r\}$ using the following equations:

$$\begin{cases}\boldsymbol{V}_r(u)=\boldsymbol{T}^{-1}(\gamma)\boldsymbol{T}^{-1}(\alpha)\boldsymbol{V}(u)=\begin{bmatrix}q_{rx} & q_{ry} & q_{rz}\end{bmatrix}^{\mathrm{T}},\\ \boldsymbol{\omega}_r(u)=\boldsymbol{T}^{-1}(\gamma)\boldsymbol{T}^{-1}(\alpha)\boldsymbol{\omega}(u)=\begin{bmatrix}\omega_{rx} & \omega_{ry} & \omega_{rz}\end{bmatrix}^{\mathrm{T}}.\end{cases} \tag{16}$$

Then eq. (9) is converted into the following equation:

$$D\cos\theta+E\sin\theta=F \tag{17}$$

with

$$\begin{cases}D=z_r(z)\left(\omega_{rx}l_{rx}+\omega_{ry}l_{ry}\right)-\left(q_{ry}l_{rx}-q_{rx}l_{ry}\right),\\ E=z_r(z)\left(\omega_{rx}l_{ry}-\omega_{ry}l_{rx}\right)-\left(q_{ry}l_{ry}+q_{rx}l_{rx}\right),\\ F=q_{rz}l_{rz}-q_{rz}z_r(z),\end{cases}$$

$$z_r(z)=\left(n_{rx}l_{rx}+n_{ry}l_{ry}\right)\Big/n_{rz}+l_{rz},$$

$$\mathrm{d}\boldsymbol{P}_r/\mathrm{d}z=\begin{bmatrix}n_{rx} & n_{ry} & n_{rz}\end{bmatrix}^{\mathrm{T}}.$$

There are two cases in solving eq. (17).

Case I: if $E\geqslant 0$

$$\theta=\operatorname{asin}\left(\frac{F}{\sqrt{D^2+E^2}}\right)-\operatorname{asin}\left(\frac{D}{\sqrt{D^2+E^2}}\right). \tag{18}$$

Case II: else if $E<0$

$$\theta=\operatorname{asin}\left(\frac{F}{\sqrt{D^2+E^2}}\right)+\operatorname{asin}\left(\frac{D}{\sqrt{D^2+E^2}}\right). \tag{19}$$

Then using eq. (6), the point on the envelope surface as well as on the rotation surface of the cutting edge can be computed. As aforementioned, the number of rotation surfaces of cutting edges is equal to the number of the cutting edges. At the height of z from the bottom of the cutter, if the radius of one of the rotation surfaces is the biggest, it is the truth that only this cutting edge, not others, contributes to the final machining accuracy at the current moment in milling. So when the cutter has more than one cutting edge, we should compute the rotation surface of each cutting edge. Then at the height of z from the bottom of the cutter, the envelope surface point on the cutting edge whose rotation radius is the maximum is chosen as the final envelope surface of the cutter.

4 Tool path optimization

In five-axis flank milling ruled surface, the fluctuations of cutting forces aroused by cutter runout is unneglectable, and compensating runout error in tool path planning will be helpful to keep milling stability. Meanwhile, the geometric error resources in flank milling can be classified into two categories. One is induced by the cutter runout effect and the other is induced by factors such as approximation error of ruled surface. When the runout effect exists, the first error resource appears. When the machined surface is non-developable ruled surface, the second error resource appears. The total error can be expressed using the following equation:

$$\varepsilon=\varepsilon_{\mathrm{non}}+\varepsilon_{\mathrm{Runout}}, \tag{20}$$

where $\varepsilon_{\mathrm{Runout}}$ is the error induced by cutter runout effect, and $\varepsilon_{\mathrm{non}}$ is the error induced by other factors.

The definition of the error ε is illustrated in Figure 8. Point $\boldsymbol{D}$ stands for a point on the machined surface. Make a line that is perpendicular to the tool path surface. This line called as the perpendicular line $\boldsymbol{n}_{\mathrm{normal}}$ intersects with the envelope surface without cutter runout effect (ideal envelope surface) at point $\boldsymbol{P}$, and intersects with the envelope surface with cutter runout effect at Point $\boldsymbol{Q}$. Then two errors in eq. (20) can be defined as

$$\begin{cases}\varepsilon_{\mathrm{Runout}}=(-1)^m\left\|\boldsymbol{Q}-\boldsymbol{P}\right\|,\\ \varepsilon_{\mathrm{non}}=(-1)^s\left\|\boldsymbol{D}-\boldsymbol{P}\right\|.\end{cases} \tag{21}$$

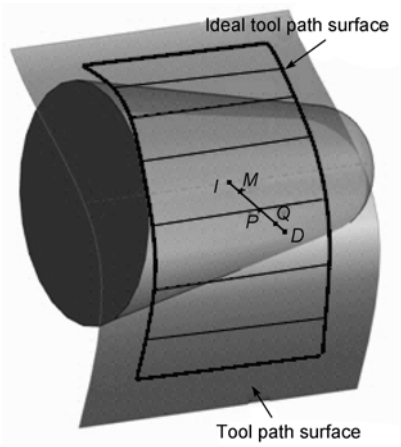

Figure 8 Error definition and map point.

The values of m and s have relationship with overcut and undercut. When the milling process is overcut, m and s are set to 1 and when the milling process is undercut, m and s can be set to 2.

The perpendicular line $\boldsymbol{n}_{\text{normal}}$ is the normal vector at some point of the tool path surface. Then the definitions of the undercut and overcut of the $\varepsilon_{\text{Runout}}$ and ε_{non} are given as follows.

For $\varepsilon_{\text{Runout}}$ when

$$\left(\frac{\partial \boldsymbol{sf}_w(u,v)}{\partial u}\times\frac{\partial \boldsymbol{sf}_w(u,v)}{\partial v}\right)\cdot(\boldsymbol{Q}-\boldsymbol{P})>0,\quad\text{(overcut).}$$

Else if

$$\left(\frac{\partial \boldsymbol{sf}_w(u,v)}{\partial u}\times\frac{\partial \boldsymbol{sf}_w(u,v)}{\partial v}\right)\cdot(\boldsymbol{Q}-\boldsymbol{P})\leqslant 0,\quad\text{(undercut).}$$

For ε_{non} when

$$\left(\frac{\partial \boldsymbol{sf}_w(u,v)}{\partial u}\times\frac{\partial \boldsymbol{sf}_w(u,v)}{\partial v}\right)\cdot(\boldsymbol{D}-\boldsymbol{P})>0,\quad\text{(undercut).}$$

Else if

$$\left(\frac{\partial \boldsymbol{sf}_w(u,v)}{\partial u}\times\frac{\partial \boldsymbol{sf}_w(u,v)}{\partial v}\right)\cdot(\boldsymbol{D}-\boldsymbol{P})\leqslant 0,\quad\text{(overcut).}$$

Using this error definition, the tool path optimization can be conducted based on the basic idea of constructing a map point. As shown in Figure 8, Point $\boldsymbol{I}$ is the projected point of $\boldsymbol{D}$ on the tool path surface. Obviously, Point $\boldsymbol{I}$ is also the intersection point between $\boldsymbol{n}_{\text{normal}}$ vector direction and tool path surface. By moving $\boldsymbol{I}$ along $\boldsymbol{n}_{\text{normal}}$ vector direction with distance $\boldsymbol{\varepsilon}$, the mapping point is got. Thus, every point on the milled surface has a mapping point. These mapping points form a mapping surface. The process of the tool path surface approaching the mapping surface is just the process of optimizing tool path.

Then the most important step is to construct optimization model of tool path. First, with eq. (8) the initial tool path surface is sampled as a series of tool axes. The corresponding mapping points of these tool axes can also be computed using the above theory. For point $\boldsymbol{I}$ on sample axis of the tool path surface, the position parameters (u, v) can be calculated. Then the error at mapping points is transformed from eq. (20) to the following equation:

$$|\varepsilon_{\boldsymbol{M}}|=\left\|\boldsymbol{M}-(1-v)\sum_{i=0}^{n}N_{i,3}(u)\boldsymbol{b}_{\text{Boti}}-v\sum_{i=0}^{n}N_{i,3}(u)\boldsymbol{b}_{\text{Topi}}\right\|.\quad(22)$$

Similarly, for all sample points on the initial tool path surface, their corresponding geometric errors can be obtained. Then tool paths are optimized by minimizing the square sum of geometric errors with respect to $\boldsymbol{b}_{\text{Boti}}$ and $\boldsymbol{b}_{\text{Topi}}$. Transforming eq. (22) to (23) and solving this equation using least squares criterion may yield the control points of improved tool path surface

$$\varepsilon_{\boldsymbol{M}}^2=\left\|\boldsymbol{M}-\left(\sum_{i=0}^{n}(1-v)N_{i,3}(u)\boldsymbol{b}_{\text{Boti}}+\sum_{i=0}^{n}vN_{i,3}(u)\boldsymbol{b}_{\text{Topi}}\right)\right\|^2.\quad(23)$$

By repeating the optimization process, the resulting errors can be further reduced using the iterative least square method.

5 Examples and discussion

The analytic model of geometric errors induced by cutter runout effect and corresponding tool path optimization method are verified using C++ language. First, the plane milling simulations with and without cutter runout are given. The radius of the cutter is 6 mm. The cutter runout is 5 μm, which is a parallel axis offset error. To compare clearly and conveniently, we assumed that the surface is milled by one cutting edge. Figure 9(a) shows the case where the plane is milled without cutter runout, and Figure 9(b) shows the case with cutter runout. It can be seen that the theoretical geometry error is zero if without cutter runout and there exists obvious theoretical geometry error if with runout. From the aspect of surface topography, no matter whether the cutter runout exists or not, both the two cases have milling microtextures. For the 5 μm runout error, the resulting magnitude of geometric errors is about 9 μm along the direction of work height. It shows that the theoretical geometry error induced by cutter runout should not be ignored. The following example is an envelope surface model and tool path planning for a curved surface milling with cutter runout. In order to have an analytic solution of envelope surface and facilitate error comparison, the tool path surface is first expressed as the following expressions without using a uniform B-spline surface.

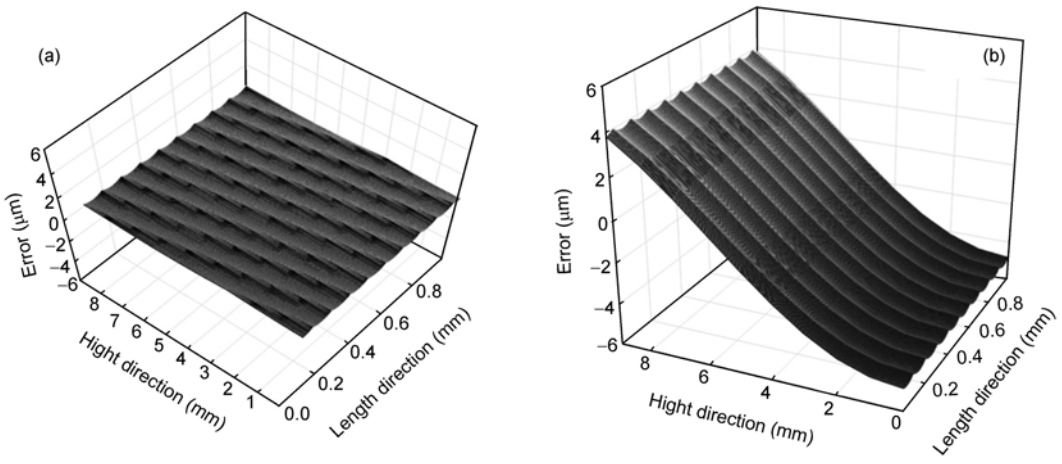

Figure 9 Plane milling with and without cutter-runout.

$$\boldsymbol{sf}(v,\phi)=v\begin{bmatrix}40\cos\phi\\40\sin\phi\\0\end{bmatrix}+(1-v)\begin{bmatrix}\left(40-20/\sqrt{3}\right)\cos\phi\\\left(40-20/\sqrt{3}\right)\sin\phi\\20\end{bmatrix}. \quad (24)$$

A flat end mill is chosen to simulate the milling process and validate the presented method. The cutter's parameters are given as follows: The radius of cutter is 6 mm, helix angle is 45 degrees, and the number of cutting edges is four. The cutting edges' equations are then transformed as

$$\begin{cases}x_c(z)=R_0\cos\left(z\tan(\beta)/R_0+2(k-1)\pi/N\right),\\y_c(z)=R_0\sin\left(z\tan(\beta)/R_0+2(k-1)\pi/N\right),\\z_c(z)=z.\end{cases} \quad (25)$$

5.1 Geometric errors induced by cutter runout

To investigate the influence of runout effect on the machining accuracy, the machined surface is given as developable ruled surface. That means the point on the machined surface is also on the ideal envelope surface of the cutter without cutter runout, and that the geometric error in milling is aroused from cutter runout effect only. Figure 10 shows the initial tool path surface and designed surface. In the validation test, if all parameters of cutter runout are set to zero, the envelope surface of cutter and the designed surface are the same. It proves that the method computing the envelope surface presented in this paper is valid.

For classifying the effects of parallel axis error and inclination angle error on geometric errors in five-axis milling respectively, two validation tests were performed first. Figure 11 shows the geometric errors induced by parallel axis error. The offset value was set to 0.006 mm and the location angle was set to 15 degrees. From Figure 11 it can be seen that the maximum geometric error aroused by parallel axis error is about equal to the magnitude of offset value. At different positions along the cutter axis direction, the magnitudes of the resulting geometric errors are also different. Also, along the workpiece direction, the shape of geometric error is almost no change. Figure 12 shows the geometric

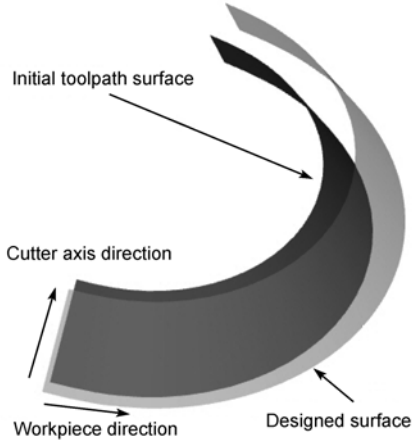

Figure 10 Initial tool path surface and designed surface.

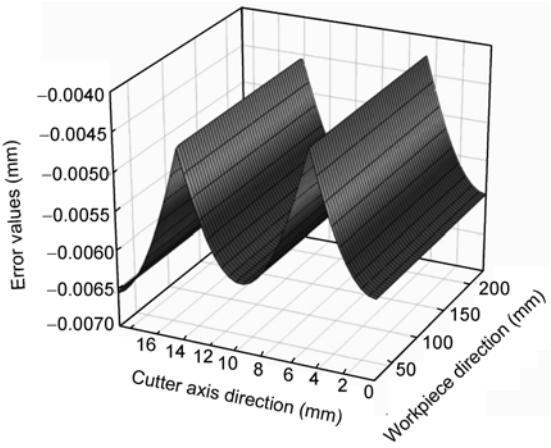

Figure 11 The errors induced by parallel axis error.

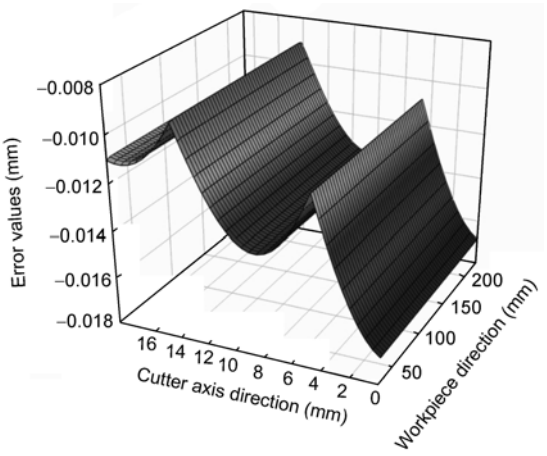

Figure 12 The errors induced by inclination angle error.

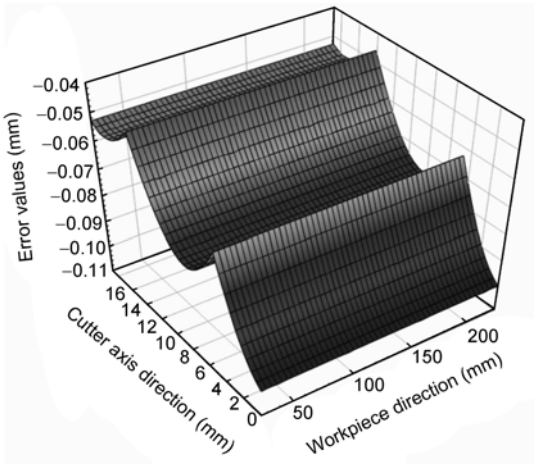

Figure 13 Error values with cutter runout effect.

errors induced by inclination angle error. The inclination angle error was set to 0.025 degree and the location angle was set to 30 degrees. From Figure 12 we can see that the geometric errors aroused by inclination angle error are different along the cutter axis direction and the magnitude of geometric error presents a declining trend with the increase of the height of cutter axis. Also we can see that the geometric error induced by inclination angle is significant and the magnitude of geometric error is dependent on the length of cutter. Under the same inclination angle error, the longer the cutter length is, the larger the geometric error becomes.

To systematically investigate the combined effect of the runout parameters on the geometric errors of the machined surface, the parallel axis error and inclination angle error were both considered in the third validation test as shown in Table 1. Figure 13 shows the geometric errors induced by the cutter runout. From this figure we can see that the errors induced by the cutter runout should not be ignored especially to ensure the inclination angle error is small enough. Another phenomenon in the figure is that the error surface has two peak lines. The reason of this is that the rotation surfaces of cutting edges are different form each other. At different heights along cutter axis, the envelope surface is constructed by the rotation surface of cutting edge whose rotation radius is the largest just like Figure 14. The number of peak lines is equal to the number of intersection lines of the outermost rotation surface of cutting edges. In Figure 14, the cutter has four edges, and the outermost surface of the rotation surface is composed of the 1st, 3rd and 4th cutting

Table 1 Cutter runout parameters

Item	Value
The offset ρ (mm)	0.005
The inclination angle γ (rad)	0.0024
The length of the cutter axis l_c (mm)	40
The location angle λ (rad)	0.0025

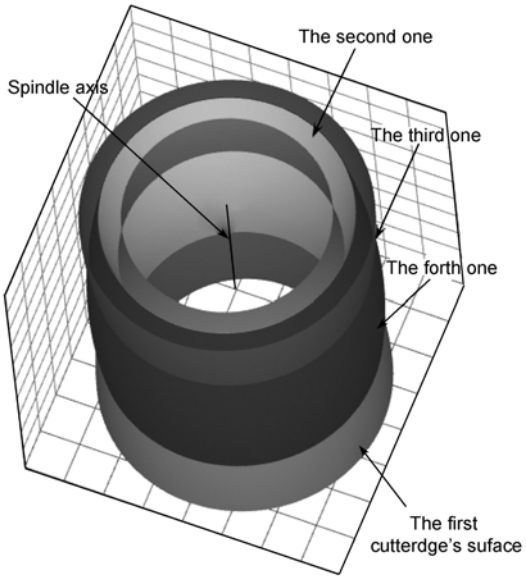

Figure 14 Rotational surface of the cutter with four edges.

edges' rotation surfaces. It means that the 2nd cutting edge's rotation surface made no contribution to the final resulting geometric errors of the machined surface and only the 1st, 3rd and 4th cutting edges played a part in this validation example due to the existence of the cutter runout effect.

5.2 Tool path optimization

For the third validation test, a tool path optimization was also conducted. According to the initial cutter location data, the tool path surface was further approximated by a B-spline surface as an initial cutter axis surface of the path optimization operation. The two curves of the B-spline ruled surface both had 19 control points. The geometric errors induced by cutter runout were first derived. Then using the optimization mode illustrated in eq. (23), the up-

dated control points of cutter axis surface were derived. The same process was repeated several times until the magnitude of geometric errors was finally reduced to a desirable level or without an obvious reduction.

Figure 15 shows the geometric error after optimizing the tool path surface. Compared with the largest error in Figure 13 it can be seen that the error is reduced significantly with a largest error reduction from 0.11 mm to 0.025 mm. The error magnitude is reduced by 77.3%. It proves that the method of optimizing tool path is effective to reduce the geometric error induced by cutter runout. After optimization, the number of peak lines in Figure 15 is equal to the number of that in Figure 13. However, the largest error without optimizing tool path lies at the bottom of cutter as illustrated in Figure 13. After optimization, the position of the largest error is at the middle part of cutter axis. Figure 16 shows a comparison of part of the tool paths before and after optimization. The right figure of Figure 16 is a partially enlarged view. From this figure, it can be seen that the cutter axis is adjusted after optimization with a largest magnitude of about 0.01 mm. It means that the geometric errors can be obviously reduced with a small cutter axis adjustment.

6 Conclusions

The analytical model of geometric errors induced by cutter runout effect is established for the first time in this paper. Then an iterative least square model is constructed to optimize the tool paths for reducing geometric errors.

1) The complete cutter runout considering parallel axis deviation and inclination angle deviation is defined with four parameters. It is helpful to systematically investigate the influence of cutter runout on the geometric accuracy of the machined surface.

2) Relative motion between the cutter and the part is analyzed with consideration of the cutter runout effect. For a tapered-helical-ball-end mill cutter, the established cutter envelope surface model has the ability to integrate with cutter runout. Through the analytical model, we found that the geometric error induced by cutter runout is significant, and that not all cutting edges make contribution to the final geometric errors of the machined surface. The influence of the runout parameters on the shape and magnitude of geometric errors in five-axis flank milling is also got.

3) A model of optimizing tool path is established. Using the iterative least square strategy, the geometric error aroused by cutter runout can be reduced significantly. Also, compensating cutter runout in tool path is helpful for reducing the fluctuations of cutting forces.

4) Validation tests have proved that the proposed computing mode of geometric errors and tool path optimization

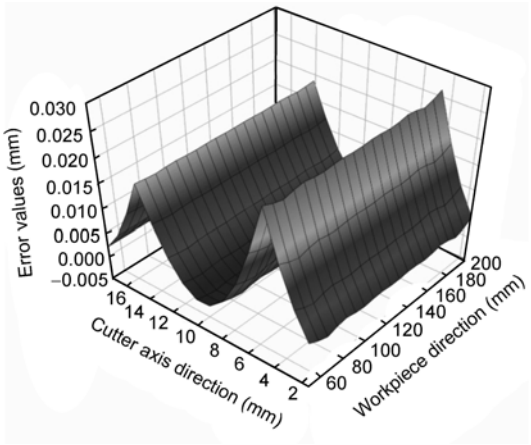

Figure 15 Error values after optimizing tool path.

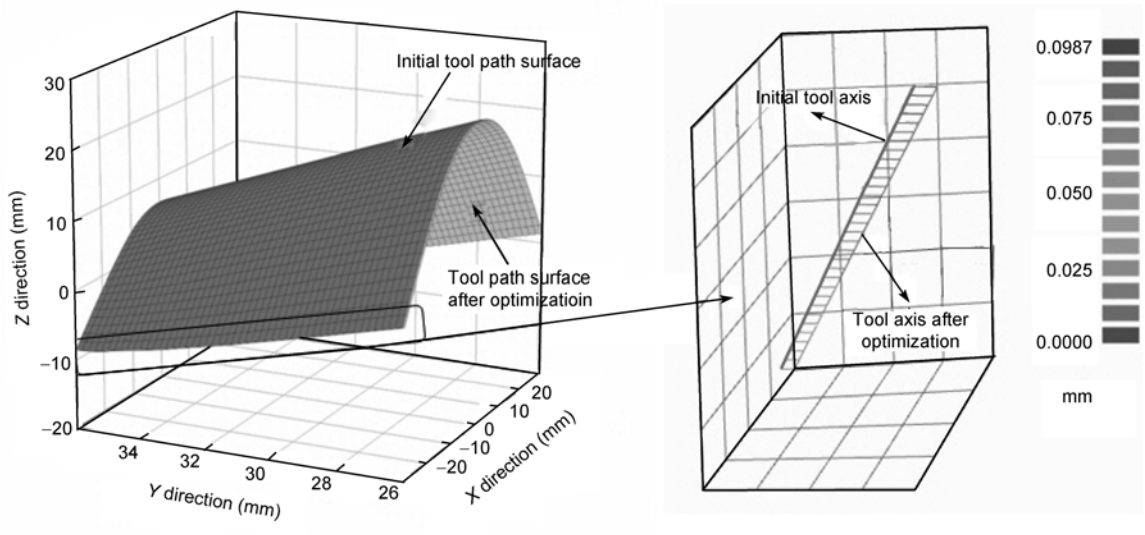

Figure 16 Cutter axis comparison before and after tool path optimization.

considering cutter runout effect is feasible and effective.

Due to the complexity of the effect of cutter runout on milling process, it is only a preliminary study and some factors such as errors of cutting edge wear and the installation of inserted tooth cutter are not taken into account in the presented runout model. These need further investigations in the future. Meanwhile, the basic assumption of the presented envelope surface model is the same as the classical assumption, namely, the effect of cutter feed on the cutter rotation surface is overlooked. If cutter runout exists, it is recommended that a good combination of process parameters such as radial depth of cut, feed per tooth and spindle speed should be given to gain a good surface quality and geometric accuracy.

This work was supported by the National Natural Science Foundation of China (Grant No. 51075054), the National Basic Research Program of China ("973" Program) (Grant Nos. 2005CB726100 and 2011CB706800) and the Fundamental Research Funds for the Central Universities (Grant No. DUT10ZD205).

1 Ding H, Zhu L M. Global optimization of tool path for five-axis flank milling with a cylindrical cutter. Sci China Ser E-Tech Sci, 2009, 53: 2449–2459
2 Gong, H, Wang N. 5-axis flank milling free-form surfaces considering constraints. Comput Aided Des, 2011, 43(6): 563–572
3 Zhu L M, Ding H, Xiong Y L. Third-order point contact approach for five-axis sculptured surface machining using non-ball-end tools (I): Third-order approximation of tool envelope surface. Sci China Tech Sci, 2010, 53: 1904–1912
4 Zhu L M, Ding H, Xiong Y L. Third-order point contact approach for five-axis sculptured surface machining using non-ball-end tools (II): Tool positioning strategy. Sci China Tech Sci, 2010, 53: 2190–2197
5 Lartigue C, Duc E, Affouard A. Tool path deformation in 5-axisflank millingusing envelope surface. Comput Aided Des, 2003, 35(4): 375–382
6 Bi Q Z, Wang Y H, Zhu L M, et al. Wholly smoothing cutter orientations for five-axis NC machining based on cutter contact point mesh. Sci China Tech Sci, 2010, 53: 1294–1303
7 Zhang X M, Zhu L M, Zheng G, et al. Tool path optimization for flank milling ruled surface based on distance function. Int J Prod Res, 2010, 48(14): 4233–4251
8 Desai K A, Agarwal P K, Rao P V M. Process geometry modeling with cutter runout for milling of curved surfaces. Int J Mach Tool Man, 2009, 49(12-13): 1015–1028
9 Sun Y W, Guo Q. Numerical simulation and prediction of cutting forces in five-axis milling processes with cutter run-out. Int J Mach Tool Man, 2011, 51(10-11): 806–815
10 Mao X Y, Liu H Q, Li Bin. Time-frequency analysis and the detecting method research on the milling force token signal in the spindle current signal. Sci China Ser E-Tech Sci, 2009, 52: 2810–2813
11 Weinert K, Du S, Damm P, Stautner M. Swept volume generation for the simulation of machining processes. Int J Mach Tool Manu, 2004, 44: 617–628
12 Zhu L M, Zhang X M, Zheng G, et al. Analytical expression of the swept surface of a rotary cutter using the envelope theory of sphere congruence. J Manuf Sci E-T ASME, 2009, 131(4): 041017
13 Larue A, Altintas Y. Simulation of flank milling processes. Int J Mach Tool Man, 2005, 45(4-5): 549–559
14 Zhang X J, Xiong C H, Ding Y, et al. Variable-step integration method for milling chatter stability prediction with multiple delays. Sci China Tech Sci, 2011, 54: 3137–3154
15 Ahmadi K, Ismail F. Machining chatter in flank milling. Int J Mach Tool Man, 2010, 50(1): 75–85
16 Wang W P, Wang K K. Geometric modeling for swept volume of moving solids. IEEE Comput Graph Appl, 1986, 6(12): 8–17
17 Sheltami K, Bedi S, Ismail F. Swept volumes of toroidal cutters using generating curves. Int J Mach Tool Man, 1998, 38(7): 855–870
18 Blackmore D, Leu M C, Wang L P. The sweep-envelope differential equation algorithm and its application to NC machining verification. Comput Aided Des, 1997, 29(9): 629–637
19 Aras E. Generating cutter swept envelopes in five-axis milling by two-parameter families of spheres. Comput Aided Des, 2009, 41(2): 95–105
20 Liu X W. Five-axis NC cylindrical milling of sculptured surfaces. Comput Aided Des, 1995, 27(12): 887–894
21 Bedi S, Mann S, Menzel C. Flank milling with flat end milling cutters. Comput Aided Des, 2003, 35(3): 293–300
22 Senatore J, Monies F D R, Redonnet J M, et al. Analysis of improved positioning in five-axis ruled surface milling using envelope surface. Comput Aided Des, 2005, 37(10): 989–998
23 Gong H, Wang N. Optimize tool paths of flank milling with generic cutters based on approximation using the tool envelope surface. Comput Aided Des, 2009, 41(12): 981–989
24 Zhu LM, Zheng G, Ding H, et al. Global optimization of tool path for five-axis flank milling with a conical cutter. Comput Aided Des, 2010, 42(10): 903–910
25 Li X P, Li H Z. Theoretical modelling of cutting forces in helical end milling with cutter runout. Int J Mech Sci, 2004, 46(9): 1399–1414